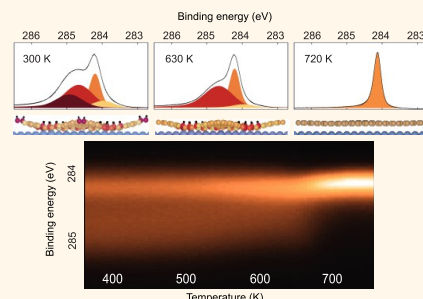


Controlling Hydrogenation of Graphene on Ir(111)

Richard Balog,^{†,*} Mie Andersen,^{†,‡} Bjarke Jørgensen,^{†,‡} Zeljko Sljivancanin,[§] Bjørk Hammer,^{†,‡} Alessandro Baraldi,[†] Rosanna Larciprete,^{||} Philip Hofmann,^{†,‡} Liv Hornekær,[†] and Silvano Lizzit[¶]

[†]Department of Physics and Astronomy and [‡]Interdisciplinary Nanoscience Center (iNANO), Aarhus University, 8000 Aarhus C, Denmark, [§]Vinča Institute of Nuclear Sciences (020), P.O. Box 522, RS-11001 Belgrade, Serbia, [¶]Physics Department and Center of Excellence for Nanostructured Materials, University of Trieste, Via Valerio 2, 34127 Trieste, Italy, and IOM-CNR Laboratorio TASC, Area Science Park, S.S.14 Km 163.5, 34149 Trieste, Italy, ^{||}CNR Istituto dei Sistemi Complessi, UOS Tor Vergata, Roma, Italy, and [¶]Elettra-Sincrotrone Trieste S.C.p.A., S.S. 14 Km 163.5, 34149 Trieste, Italy

ABSTRACT Combined fast X-ray photoelectron spectroscopy and density functional theory calculations reveal the presence of two types of hydrogen adsorbate structures at the graphene/Ir(111) interface, namely, graphane-like islands and hydrogen dimer structures. While the former give rise to a periodic pattern, dimers tend to destroy the periodicity. Our data reveal distinctive growth rates and stability of both types of structures, thereby allowing one to obtain well-defined patterns of hydrogen clusters. The ability to control and manipulate the formation and size of hydrogen structures on graphene facilitates tailoring of its properties for a wide range of applications by means of covalent functionalization.



KEYWORDS: graphene · Ir(111) · hydrogen · XPS · DFT

Graphene has potential to be used in a variety of applications such as protective coatings,¹ transparent electrodes,² terahertz electronic devices,^{3,4} rapid DNA sequencing,⁵ and selective gas detectors,^{6,7} to name just a few. However, in many of the proposed applications, the intrinsic properties of graphene need to be modified. Functionalization of graphene by attaching simple atomic species such as O,^{8,9} F,¹⁰ and H^{4,11–15} allows for limited control over the transformations required by such diverse applications. As a result, a great deal of research aims at modifying graphene with larger functional groups, thereby achieving richer functionality and better control over graphene properties. Recently, two interesting approaches have been proposed to simplify the overall functionalization process. While the first one predicts a lower adsorption barrier of functional groups simply by applying strain to the graphene sheets,¹⁶ the second requires preactivation of the basal plane of graphene with hydrogen followed by chemical treatment.¹⁷ Here, the aim is to achieve complete control over processing with hydrogen

since the functionalization in the second step selectively acts only on hydrogenated areas. The advantage of the latter approach is that by achieving patterned hydrogenation one may easily overcome difficulties imposed by treatment with radicals in wet chemistry approaches, where direct anchoring of larger species to otherwise inert graphene often results in ill-defined functionalized layers. For this reason, covalent functionalization, at present, is mostly used in connection with wet exfoliation techniques aimed at cheap mass production of graphene from graphite.¹⁸

Hydrogenation of graphene has also attracted considerable attention due to the possibility to control the electronic properties of graphene. To be able to use graphene as a base material in the semiconductor industry, one needs to alter its intrinsic metallic behavior into that of a semiconductor. Bonding of atomic hydrogen to graphene has been shown to open the gap at the Dirac point,¹² which is the prerequisite for obtaining the required behavior. Recent studies have even shown that the size of the gap can be tuned by controlling the extent of hydrogenation.^{19,20}

* Address correspondence to balog@phys.au.dk.

Received for review September 10, 2012 and accepted April 15, 2013.

Published online April 15, 2013
10.1021/nn400780x

© 2013 American Chemical Society

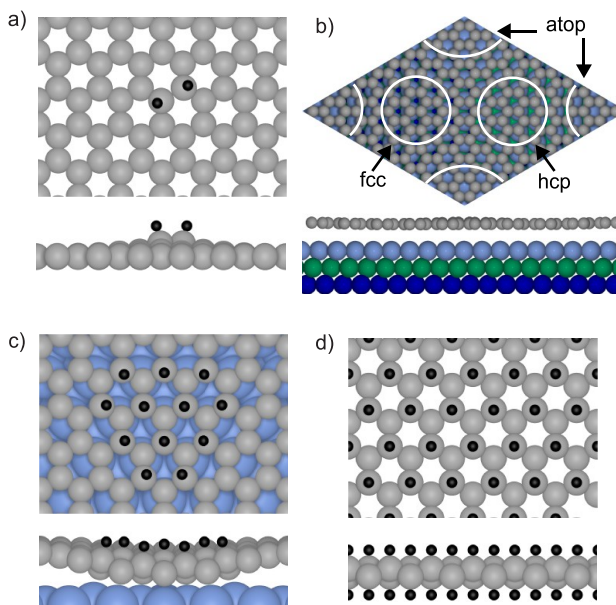


Figure 1. Examples of various hydrogen structures formed on a graphene sheet. (a) Hydrogen dimer. (b) Definition of distinct regions of the moiré supercell formed on the graphene/Ir(111) interface due to lattice mismatch. In hexagonal close-packed (hcp) and face-centered cubic (fcc) regions, every second carbon atom is positioned above an iridium atom, while every other second carbon atom is positioned above a hollow site. Hcp and fcc regions differ only by the type of hollow site below the carbon atoms (fcc or hcp). In atop regions, all carbon atoms are positioned above hollow sites. (c) Graphane-like structure: every second carbon within the hexagon has attached hydrogen on the upper side of the graphene, while every other second carbon is bound to the substrate. Such a configuration is possible only on the hcp and fcc parts of the graphene/Ir(111) interface. (d) Graphane: every second carbon within the hexagon has attached hydrogen on the upper side of the graphene, while every other second carbon has attached hydrogen from the lower side.

The reaction of atomic hydrogen with a hexagonal sp^2 carbon network such as an HOPG surface has already been extensively studied^{21–25} and in short can be summarized as follows: the long-range attractive interaction between impinging atomic hydrogen and a carbon atom destabilizes the planar hexagonal configuration by pulling one carbon atom in an out-of-plane direction. The shifting of a carbon atom out of the plane has a barrier of about 0.15–0.2 eV.^{21,25} Thus, the impinging hydrogen must possess enough kinetic energy to overcome the adsorption barrier, break the $C=C$ double bond, and create a single C–H bond. As the result, the carbon atom binding the hydrogen changes its hybridization from sp^2 to sp^3 . Such a strong chemical and configurational modification reflects in the corresponding C 1s core level spectrum.²⁶ Since bond cleavage by a single hydrogen atom leads to the formation of a monomer (i.e., only one C–H bond), the process leaves an unpaired electron on a neighboring carbon atom. This system is metastable at room temperature and tends to release hydrogen and re-form the double bond. However, if within the lifetime of the monomer another hydrogen atom binds to the dangling bond, it will create a dimer (see Figure 1a). Dimers have been found to be the most stable structures on HOPG.^{21,22,27}

The reaction of atomic hydrogen with graphene, on the other hand, appears to be strongly influenced by the underlying substrate. As mentioned above, the two neighboring carbon atoms need to be saturated in

order to achieve the most stable structures.^{21,22,28} We consider at first the case of graphene on a SiC substrate, where the interaction is very weak. Exposure of graphene to atomic hydrogen has been observed to result in the formation of dimer structures¹¹ similar to those found on HOPG. Therefore, from a chemical point of view, the graphene on SiC resembles the topmost HOPG layer. Despite the very similar behavior of the two substrates, a slight difference has been observed. Due to a topological corrugation of the graphene on SiC, preferential adsorption of hydrogen on the convex areas has been revealed at very low hydrogen coverage.¹¹ This is because convex (concave) areas effectively reduce (increase) the initial barrier for hydrogen adsorption with the effect being more pronounced for higher curvature.^{29,30} Since the curvature of the corrugated areas in graphene/SiC is relatively small,³¹ the apparent preferential adsorption vanishes with increasing hydrogen coverage.

The reaction of hydrogen with graphene is more strongly affected by the presence of transition metal substrates. For example, hydrogen structures on graphene/Ir(111)¹² and graphene/Pt(111)³² were observed to follow the moiré superstructure even at relatively high hydrogen coverage.

The corrugation of the graphene sheet on both metal substrates cannot account for preferential adsorption, and this becomes even more evident if we consider some general characteristics of these systems. Taking graphene/Ir(111) as an example, one finds that

despite the weak interaction between the graphene and iridium substrate,^{33,34} recent calculations have revealed slightly stronger binding between C and Ir atoms in hexagonal close-packed (hcp) and face-centered cubic (fcc) regions of the moiré superstructure as compared to atop regions.³⁵ Figure 1b defines the different regions. The difference originates from the stronger interaction between the C atoms positioned just above the Ir atoms, a configuration that is not present in the atop regions, but takes place for every second C atom within the hexagon in hcp and fcc regions, only. Such a configuration may drive the formation of a direct C–Ir bond upon hydrogen adsorption on the opposite side of graphene, as proposed in ref 12. In this way, one achieves the so-called graphane-like hydrogen structures (Figure 1c). The name derives from the structural similarity to graphane where all of the carbon atoms are hydrogenated in an alternating way on both sides of the graphene sheet^{36,37} (Figure 1d). Graphane-like structures have recently been proposed to form in hydrogenated graphene on various transition metal substrates.^{1,12,14,19,32,38}

In this article, we present a thorough investigation of the formation and thermal stability of the hydrogen structures on the graphene/Ir(111) interface by means of fast X-ray photoelectron spectroscopy (XPS) and density functional theory (DFT) calculations. We have monitored *in situ* the evolution of the C 1s and Ir 4f_{7/2} core levels during hydrogenation and dehydrogenation of graphene in order to follow the modality of H adsorption and desorption with H₂ recombination. DFT calculations have been used to investigate different arrangements of the H atoms, and the corresponding C 1s binding energy (BE) shifts were compared to the experimental results. Two major H cluster configurations are detected, namely, graphane-like islands and hydrogen dimers.¹²

RESULTS AND DISCUSSION

The top panels in Figure 2a,b show the Ir 4f_{7/2} and the C 1s spectra, respectively, measured for the clean graphene/Ir(111) interface. While the C 1s spectrum consists of a single component (C_c) positioned at a binding energy of 284.12 eV, the Ir 4f_{7/2} comprises two components due to bulk (B) and first layer Ir atoms (S) at 60.84 and 60.31 eV, respectively. The resemblance of the Ir 4f_{7/2} core level spectrum with that of a bare iridium substrate (not shown) is a consequence of the very weak interaction between graphene and the Ir(111) substrate.^{39,40}

Exposure of graphene to a hot atomic hydrogen beam causes drastic changes in both the Ir 4f_{7/2} and the C 1s line shapes. To visualize the changes occurring during hydrogen dosing, the core level spectra acquired by fast XPS during the hydrogen uptake at room temperature are shown as two-dimensional intensity plots in the central panels of Figure 2a,b, while the

bottom panels of the same figure show the Ir 4f_{7/2} and the C 1s spectra taken on the surface at saturation. Hydrogenation causes a significant reduction of the S component in the Ir 4f_{7/2} spectrum, accompanied by the appearance of a new component, G at a BE of 60.62 eV. The behavior of the intensity of these two components as a function of the H dose, as derived from the analysis of the fast XPS data and shown in Figure 2c, clearly points toward a transformation of S into G during hydrogenation, starting already at very low hydrogen coverage. Furthermore, the evidence that at saturation coverage the S intensity has only halved implies that a large fraction of the Ir surface atoms remains unperturbed by the hydrogenation process. The strong influence of hydrogenated graphene on the substrate surface component has also been reported for Pt(111)^{14,32} and Ni(111).¹⁴

As seen in Figure 2b, atomic hydrogen adsorption onto graphene also has a significant influence on the C 1s spectrum. The initial sp² peak (C_c) loses its intensity, while a distinct broad feature emerges at higher BE. The C 1s spectrum taken on the hydrogen-saturated surface exhibits, in addition to the C_c component, three new components marked as C_a, C_b, and C_d positioned at 284.99, 284.62, and 283.91 eV, respectively. The final position of the C_c peak is shifted by about 65 meV to higher BE. All components have relatively broad line shapes, indicating that each one includes contributions from C atoms in various configurations or differently affected by H adsorption. The details of the C 1s analysis are reported in the Supporting Information. The intensities of all of the components *versus* hydrogen dose are shown in Figure 2d. Interestingly, in the first stage of H adsorption, only the component C_b starts to develop, while at higher hydrogen dose, C_a and C_d grow shortly after each other. In parallel, the intensity of the component C_c decreases to ~30% of its initial value, indicating that relatively large parts of the graphene sheet still remain sp²-hybridized. This result suggests that the complete hydrogenation of graphene (*i.e.*, to achieve a C/H ratio of 1:1 as in graphane) is not possible for this system.

The thermal stability of the hydrogenated graphene was studied by annealing the H-saturated surface up to 820 K at a constant heating rate of 0.2 K/s while acquiring the C 1s and Ir 4f_{7/2} spectra. The corresponding two-dimensional intensity plots are shown in the central panels of Figure 3a,b, whereas the intensities of the Ir 4f_{7/2} and C 1s components as a function of the temperature are reported in Figure 3c,d. The changes in the Ir 4f_{7/2} spectrum occur at relatively high temperature and are related to the transformation of G back to S (Figure 3c). The threshold for the conversion is at about 620 K, though the S intensity is only fully recovered at ~720 K. In contrast to Ir 4f_{7/2}, the behavior of the C 1s spectrum with thermal annealing provides a strong indication for the coexistence of various types of hydrogen structures (Figure 3d). The difference in

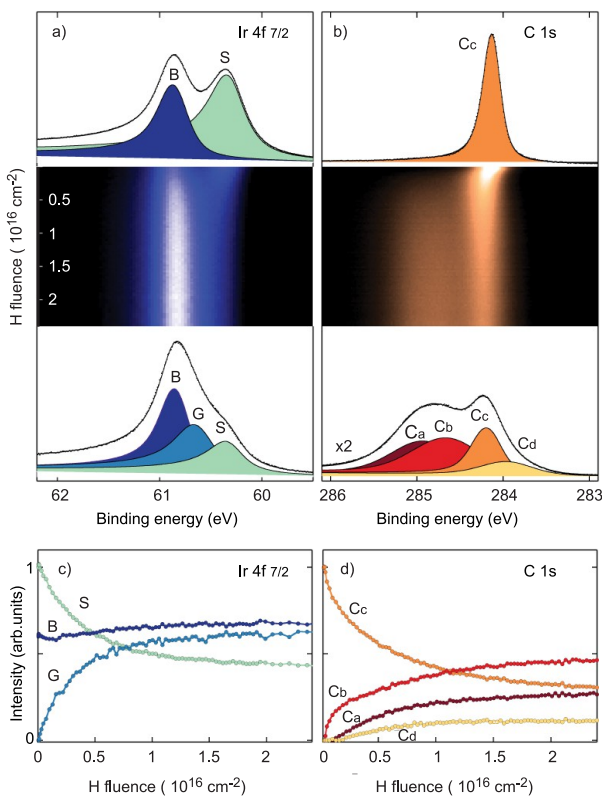


Figure 2. Ir 4f_{7/2} and C 1s core level spectroscopy during H uptake on graphene/Ir(111). (a,b) Core level spectra measured on the clean graphene/Ir(111) surface (top) and on the same surface saturated with H (bottom). The B and S components are due to bulk and first layer atoms in the iridium substrate while the C_c component represents the sp²-hybridized C atoms in graphene. The central panels display the 2D plots of the fast XPS spectra measured while dosing hydrogen on graphene at room temperature. The G component in the Ir 4f_{7/2} and the C_b and C_d components in the C 1s spectrum are due to the formation of graphane-like clusters. The C_a component in the C 1s spectrum is due to hydrogen dimer structures and/or isolated monomers at the periphery of the graphane-like cluster (see text). (c,d) Evolution of Ir 4f_{7/2} and C 1s component intensities (normalized to the highest intensity component) vs hydrogen dose.

the thermal behavior of the various C 1s components can in short be summarized as follows: C_a is the least stable component as it vanishes gradually between ~400 and ~630 K. C_b and C_d begin to decrease at higher temperatures. However, while the component C_d vanishes completely at ~680 K, the most stable component C_b is present up to 720 K. At this temperature, the C_c component (*i.e.*, the clean graphene) has also fully recovered its intensity, in close agreement with the recovery of the S component in the Ir 4f_{7/2} spectrum. The Ir 4f_{7/2} and C 1s spectra measured on the annealed surface are similar to those measured before the hydrogenation. This demonstrates that, independently of the type of hydrogen structures which form at the surface, hydrogenation of graphene on Ir(111) is fully reversible. This behavior is in strong contrast to graphene exposure to atomic oxygen, where thermal annealing results in etching of large graphene areas.^{8,9}

On the basis of the observations above, the modified interaction between hydrogenated graphene and iridium indicated by the appearance of the G component in the Ir 4f_{7/2} spectrum is assigned to the formation of graphane-like clusters. The reaction of hydrogen with graphene breaks the π conjugation in

the graphene layer, which subsequently allows for the formation of a stable bond between an unsaturated carbon and an iridium atom, hence the G component in the Ir 4f_{7/2} spectrum. By comparing the growth behavior and thermal stability of G with all C 1s components, one observes a similar behavior for the C_b component only; that is, both G and C_b form at the early stage of the hydrogenation (Figure 2c,d) and display the same behavior with temperature (Figure 3c,d).

In the following, we will assign all C 1s components to various hydrogen structures by direct comparison of the experimental core level shifts (CLSs) with those calculated by DFT for various hydrogen configurations on graphene/Ir(111). The CLSs are found to be strongly dependent on the size of the H cluster, the relative position of the carbon atoms within the cluster, and their chemical environment. Therefore, performing the assignment of the C 1s components just considering one arbitrary hydrogen cluster as used in refs 19 and 32 may lead to an incomplete picture. We start with graphane-like structures which are compact and defect-free. Figure 4a,b depicts these structures and the corresponding C 1s CLSs for small and large

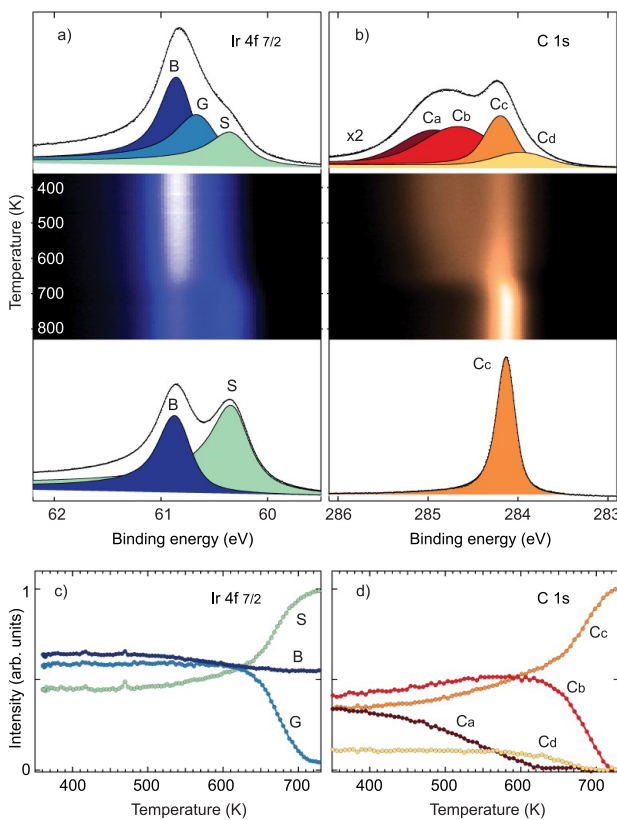


Figure 3. Ir 4f_{7/2} and C 1s core level spectra during thermal annealing of the hydrogenated graphene/Ir(111). (a,b) Core level spectra measured before (top) and after (bottom) heating the sample to 830 K. The central panels display the 2D plots of the fast XPS spectra measured while annealing the sample. (c,d) Evolution of Ir 4f_{7/2} and C 1s component intensities (normalized to the highest intensity component) vs temperature.

H coverage, respectively. These graphane-like clusters are very stable with an average binding energy per H atom of 1.49 and 2.20 eV for the small and large clusters, respectively, in good agreement with the results of ref 38. Carbon atoms bound to Ir after the chemisorption of H tend to have negative CLSs, getting progressively more negative as the H cluster grows. For carbon bonded to H, positive CLSs are found in small clusters and in the periphery of the large clusters while negative shifts are found inside the large clusters. Altogether, assuming uniform hydrogen islands, the CLSs cover energies between ~ 0.5 and -1 eV. Consequently, in addition to the component C_b, also the component C_d is assigned to originate from the graphane-like environment. Surprisingly, small graphane-like clusters have a tendency to contribute to positive CLSs only, save the central carbon atoms bound to Ir within the cluster (Figure 4a). Clusters of larger size, however, give both positive and negative shifts (Figure 4b). This suggests that at low coverage the component C_b should largely dominate over C_d, while the component C_d would only be visible at high hydrogen dose. This behavior is indeed consistent with our experimental data where C_d is seen to emerge only at a higher coverage (Figure 3c). The distribution of CLSs within small and large clusters can also explain the disappearance of C_d at slightly lower temperature

than C_b during the thermal annealing (Figure 3d). With increasing temperature, weakly bound H atoms at the periphery of the clusters are expected to desorb first. The disappearance of the C_d component can then be related to shrinkage of the average cluster to a size where positive shifts dominate again. In fact, if one relates the intensity of the C_b component with the average size of the graphane-like clusters, it becomes evident that component C_d emerges and vanishes, respectively, at very similar values of the C_b component, hence at similar cluster size during hydrogen deposition and annealing. Note also that the disappearance of the C_d component at ~ 680 K excludes that C_d originates from defects or graphene edges, as reported in ref 32.

While DFT calculations clarify the behavior of the CLSs in going from small to large clusters and vice versa, there is only poor agreement between the calculated and experimental C 1s line shapes of graphane-like clusters. Comparing the experimental C 1s spectrum measured on H/Gr/Ir(111) at saturation coverage (Figure 2b) with the C 1s spectrum calculated for high H coverage (Figure 4b), it is apparent that the part between -0.5 and -1 eV calculated for Ir-bound carbon atoms is absent in the experimental spectrum, which instead shows a higher intensity at BE ~ 1 eV higher than that of the component C_c. The experimental

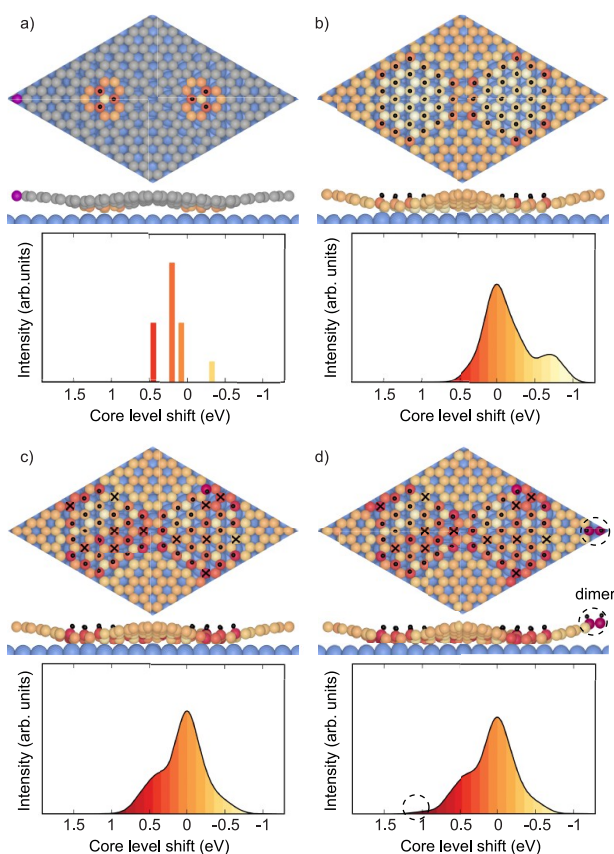


Figure 4. Calculated structures and C 1s CLSs of graphane-like clusters in the fcc and hcp regions on graphene on Ir(111) at (a) low coverage, (b) high coverage, (c) high coverage with vacancies, and (d) high coverage with vacancies and a hydrogen dimer in the atop region. Top views and side views (top) and corresponding calculated core level shifts (bottom). Ir atoms are blue, H atoms are black, and C atoms are gray or colored according to their CLS from yellow (negative CLS) to red (positive CLS). The purple atom is used as reference at low coverage. Black crosses in (d) denote hydrogen vacancies.

data and the calculations can be brought into better agreement by considering hydrogen vacancies within the graphane-like clusters. Figure 4c shows the structure and calculated CLSs of graphane-like H clusters at high coverage with some H atoms selectively removed from different places in the cluster. The introduction of H vacancies causes the average binding energy per H atom to decrease from 2.20 to 2.16 eV. As can be seen in the figure, due to the disruption of the perfect graphane-like structure, the C 1s CLSs now span an energy range from +0.7 to -0.5 eV, in closer agreement with the experiment. Furthermore, there are a few H atoms at the periphery with C atoms in these positions having larger positive shifts between 0.6 and 0.7 eV (the darkest carbon atoms in Figure 4c). These C atoms may, therefore, contribute to the component C_a , though the stability of those hydrogens at room temperature is questionable. In addition, after introducing vacancies, there is an evident tendency to differentiate between carbon atoms bonded to hydrogen (positive shift) and to iridium (negative shifts). The imperfect hydrogen cluster introduced in calculation appears realistic since hydrogen vacancies may easily form in the course of cluster growth by adsorption of hydrogen into random positions and/or by Eley–Rideal H abstraction reactions,

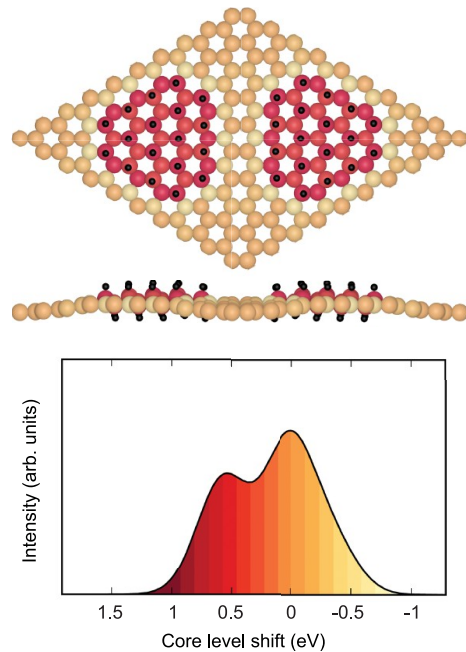


Figure 5. Calculated structure and C 1s CLSs for graphane clusters. Graphane clusters have been positioned at the fcc and hcp regions of the moiré supercell. CLSs show similar behavior as the graphane-like clusters with hydrogen vacancies included (Figure 4c).

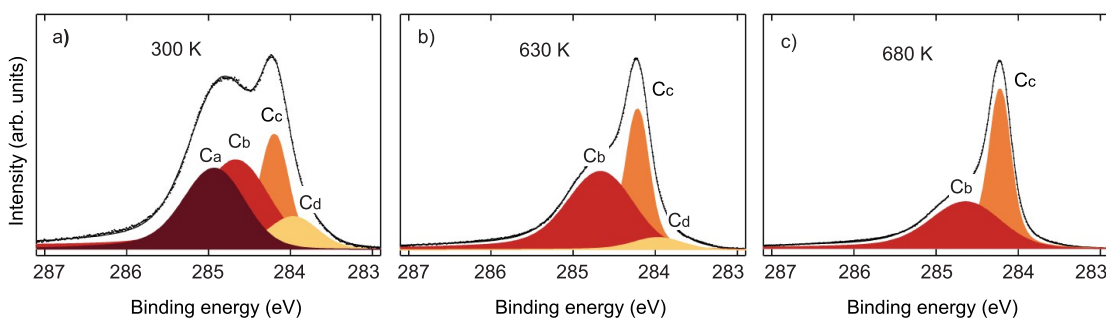


Figure 6. (a) Fitted C 1s core level spectra for hydrogen-saturated graphene at 300 K. Two main hydrogen structures are observed, namely, dimers—detected by the presence of the C_a component and graphane-like clusters detected by the presence of C_b and C_d components. (b) Hydrogen-saturated graphene after annealing to 630 K. Dimer structures have been removed from the surface, leaving vacant graphane-like clusters on fcc and hcp areas. (c) After annealing hydrogenated graphene to 680 K, graphane-like clusters become smaller in size as seen by the disappearance of the C_d component and the reduction of the C_b component.

with the latter process being important at higher hydrogen coverage.⁴¹ Though the cross section for hydrogen abstraction reactions is not known for the present system, H_2 formation is exothermic by about 2 eV and thus may produce vacancies.

While isolated hydrogen atoms on graphene could originate a contribution to the least stable component C_a , other and possibly more dominant contributors to C_a are carbon atoms influenced by hydrogen dimer structures. Indeed, calculated CLSs for the C 1s spectrum of the hydrogenated graphene including hydrogen dimers, as depicted in Figure 4d, show components at BEs positioned ~ 1 eV above the C_c peak. Furthermore, the thermal stability of C_a depicted in Figure 1d resembles that of hydrogen dimer structures on HOPG.⁴² The high positive CLS values associated with the H dimers are partly caused by the increased graphene distance to the substrate due to buckling induced by the dimer structures. The introduction of dimers lowers the average binding energy per H atom of the structure in Figure 4d to 2.13 eV since dimers are generally less stable than graphane-like clusters. The dimers are expected to form only in the atop region of the graphene/Ir(111) interface because there the bonding to the metal, and thereby the formation of graphane-like clusters, is not energetically favorable. Consequently, dimers tend to destroy the periodic hydrogen pattern formed by the graphane-like clusters in the hcp and fcc regions. The existence of a minority population of dimer structures on hydrogenated graphene on Ir(111) is in accord with recent sum-frequency generation spectroscopy measurements.⁴³ One should also note that, in addition to dimers, in ref 43, the formation of graphane structures was revealed, meaning that hydrogen binds at both sides of the graphene sheet. Our calculations show that the C 1s components for graphane clusters on free-standing graphene and vacant graphane-like structures would be very similar (see Figures 4c and 5). Therefore, we cannot exclude that some graphane structures can form during the hydrogenation.

Our study reveals that, at low coverage, hydrogen populates exclusively graphane-like states in the hcp and fcc regions of graphene/Ir(111), as evident from Figure 2d. Though this finding is in line with our previous STM studies,¹² the observed formation of hydrogen structures at specific regions is not *a priori* expected. Primarily, one would assume simultaneous formation of both types of hydrogen structures covering the whole moiré supercell at random rates. Since an already chemisorbed hydrogen cannot diffuse along the surface²² and thus allow hydrogen accumulation at certain regions, the observed preferential adsorption must be due to other effects. The possible explanation is the increased presence of monomers in the fcc and hcp regions favored by the enhanced stability of a monomer and/or the lower barrier for the formation of a monomer in hcp and fcc regions. In order to support this hypothesis, we calculated the binding energy for a hydrogen monomer adsorbed in the hcp and in the atop region. In both cases, we chose to adsorb the hydrogen atom on a carbon atom positioned in a hollow site with respect to the iridium surface lattice. Since van der Waals forces are expected to dominate the graphene/Ir(111) interface at very low hydrogen coverage, these calculations were performed using the M06-L functional. For the hcp region, we get a binding energy of 1.01 eV, whereas in the atop region, the binding is lowered to 0.89 eV. This difference can be explained by the charge transfer arguments in hcp and fcc regions as mentioned in the introduction.³⁵ The increased stability of a monomer on hcp and fcc parts would then consequently lead to an increased amount of nucleation sites on those regions from which larger graphane-like clusters can grow faster.

Another important finding is that the graphane-like clusters can be formed on graphene/Ir(111) not only by dosing the proper amount of H atoms at low temperature but also by annealing a saturated layer above 630 K (Figure 6a,b). Indeed, at this temperature, the component C_a associated with dimer structures formed in atop regions, and possibly also with isolated

hydrogenated carbon atoms at cluster edges disappears completely. This gives the unique opportunity to obtain hydrogenated regions with better defined structure than those prepared at room temperature. In addition, one can continuously change the size of the graphane-like regions by properly selecting the annealing temperature and time as observed by the disappearance of the component C_d in Figure 6c. This should result in a continuous tuning of the band gap at the Dirac point as predicted in ref 12.

CONCLUSION

In summary, we have obtained a detailed understanding on the formation and stability of two distinct types of hydrogen structures on the graphene/Ir(111)

interface, namely, dimers and graphane-like islands. This was possible by combining fast XPS measurements with DFT calculations. We have revealed apparent preferential adsorption of hydrogen on hcp and fcc parts of the moiré superstructure at low hydrogen coverage due to the influence of the local environment. Furthermore, graphane-like clusters in the hcp and fcc regions are shown to be more stable than the other hydrogenated parts, thus opening the possibility to pattern the graphene layer with size-selected hydrogen structures by thermal annealing of a saturated layer. The ability to control the hydrogenated areas at the nanometer scale may have large implications for tuning the band gap in graphene as well as for tailoring the properties of graphene with large functional groups.

METHODS

The experiments were performed in the ultrahigh vacuum chamber (base pressure 8×10^{-11} mbar) of the SuperESCA beamline at the Elettra synchrotron radiation facility (Trieste, Italy). The Ir substrate was prepared by cycles of Ar^+ sputtering at 1.5 keV, oxygen treatment between 600 and 1000 K, and flash annealing at 1473 K. Temperatures were measured via a K-type thermocouple spot-welded to the edge of the crystal. The heating of the sample is controlled by W filament positioned on the back of the sample at a distance of a couple millimeters. Temperatures above 900 K are achieved by electron bombardment with sample biased positively. The sample quality was checked both with low-energy electron diffraction, providing an intense moiré pattern for a clean graphene monolayer, and with photoemission from the C 1s and the Ir 4f_{7/2} core levels. Graphene was grown by ethylene (C_2H_4) pyrolysis in several cycles consisting of saturating the surface at 620 K followed by flash annealing to 1423 K, followed by a prolonged annealing at high temperature with a base ethylene pressure of 1×10^{-7} mbar. A hot atomic hydrogen beam was generated by cracking H_2 in a 2100 K hot tungsten capillary. The sample was kept at room temperature and exposed to atomic hydrogen for increasing time. The hydrogen exposures are given in atomic hydrogen fluence given the H flux at the sample surface of about 3×10^{14} atoms/cm² s at a base molecular hydrogen pressure of the order of $\sim 10^{-8}$ mbar. The absolute uncertainty of the flux is estimated to be within factor 3. For the thermal desorption experiments, the sample was heated at 0.2 K/s while acquiring Ir 4f_{7/2} and C 1s spectra by fast XPS. For fast XPS measurements, the time to acquire the spectrum was ~ 11 s for C 1s and ~ 8 s for Ir 4f_{7/2}, with a total acquisition time of approximately 15 min for H uptake and 20 min for TPD experiments. During the fast XPS measurements, the sample is grounded and no influence on the XPS spectra due to filament heating has been observed in that case. Alternatively, the sample was heated in steps, and each time, high-resolution photoemission spectra were acquired at room temperature.

Ir 4f_{7/2} and C 1s core level spectra were measured at photon energies of 130 and 400 eV, respectively, with an overall energy resolution ranging from 40 to 60 meV. For each spectrum, the binding energy was calibrated by measuring the Fermi level position of the Ir substrate. The measurements were performed with the photon beam impinging at grazing incidence (70°), while photoelectrons were collected at a normal emission angle. The core level spectra were fitted using Doniach-Šunjić functions convoluted with Gaussians and a linear background.

The calculations were performed with the real-space projector augmented wave GPAW code⁴⁴ using either the PBE⁴⁵ or the M06-L functional⁴⁶ for describing exchange and correlation. The

PBE functional is known to underestimate van der Waals interactions, but in ref 38, it was shown to correctly predict geometries and binding energies for H adsorption on graphene on weakly interacting transition metal surfaces, except at very low coverage (1–2 H atoms). Therefore, all monomer calculations were performed with the M06-L functional, whereas the CLS calculations at higher coverage were performed with the PBE functional for reasons of computational efficiency. It was checked that the M06-L functional gives similar results for these systems. The Ir–graphene interface was modeled with a (10 × 10) graphene sheet on a three-layered (9 × 9) Ir(111) surface, which is very close to the experimentally observed incommensurate moiré unit mesh of (10.32 × 10.32) graphene lattice vectors to (9.32 × 9.32) Ir lattice vectors.⁴⁷ Two-dimensional periodic boundary conditions were employed parallel to the slab, and a vacuum region of 6 Å separated the slab from the cell boundaries perpendicular to the slab. The graphene lattice constant was fixed to its optimized value of 2.467 Å with PBE and 2.450 Å with M06-L, and the metal lattice constants were adapted accordingly. Only the Γ point was used to sample the Brillouin zone. The grid spacing was 0.20 Å with PBE and 0.18 Å with M06-L.

For calculating the core level shifts (CLSs), the fully screened core hole approximation was used, meaning that the self-consistent total energy of the system including the core hole was evaluated, thus including final state effects. A carbon atom in the clean area of the graphene was used as the reference for the calculations at low coverage. At high coverage, the CLSs of all 200 carbon atoms were calculated and the peaks were broadened with a Gaussian of fwhm 0.3 eV for the graphane-like clusters and 0.5 eV for the graphene clusters to mimic the experimental spectrum. At high coverage, the reference was given as the point of highest intensity, which ensured that the reference point is in accordance with the position of the fitted peak corresponding to the clean area of graphene in the experimental spectrum. With the used sign convention, a positive CLS corresponds to a shift to higher binding energies in the experiment.

Conflict of Interest: The authors declare no competing financial interest.

Acknowledgment. We acknowledge financial support from the European Research Council under ERC starting grant "HPAH", No. 208344, from the Danish Council for Independent Research, Natural Sciences, from the Danish Council for Independent Research, Technology and Production Sciences, and from the Lundbeck Foundation. A.B. acknowledges the Università degli Studi di Trieste for the Finanziamento per Ricercatori di Ateneo and the MIUR under the program PRIN2010-2011 for the project "GRAF. Frontiers in Graphene Research:

understanding and controlling Advanced Functionalities". R.L. thanks the support of the COST Action MP0901 "NanoTP".

Supporting Information Available: Description of obtaining C 1s components at various temperatures. This material is available free of charge via the Internet at <http://pubs.acs.org>.

REFERENCES AND NOTES

- Nilsson, L.; Andersen, M.; Balog, R.; Laegsgaard, E.; Hofmann, P.; Besenbacher, F.; Hammer, B.; Stensgaard, I.; Hornekaer, L. Graphene Coatings: Probing the Limits of the One Atom Thick Protection Layer. *ACS Nano* **2012**, *6*, 10258–10266.
- Bonaccorso, F.; Sun, Z.; Hasan, T.; Ferrari, A. C. Graphene Photonics and Optoelectronics. *Nat. Photonics* **2010**, *4*, 611–622.
- Wang, Z.; Zhang, Z.; Xu, H.; Ding, L.; Wang, S.; Peng, L.-M. A High-Performance Top-Gate Graphene Field-Effect Transistor Based Frequency Doubler. *Appl. Phys. Lett.* **2010**, *96*, 173104.
- Yang, H.; Heo, J.; Park, S.; Song, H. J.; Seo, D. H.; Byun, K. E.; Kim, P.; Yoo, I.; Chung, H. J.; Kim, K. Graphene Barristor, a Triode Device with a Gate-Controlled Schottky Barrier. *Science* **2012**, *336*, 1140–1143.
- Schneider, G. F.; Kowalczyk, S. W.; Calado, V. E.; Pandraud, G.; Zandbergen, H. W.; Vandersypen, L. M. K.; Dekker, C. DNA Translocation through Graphene Nanopores. *Nano Lett.* **2010**, *10*, 3163–3167.
- Schedin, F.; Geim, A. K.; Morozov, S. V.; Hill, E. W.; Blake, P.; Katsnelson, M. I.; Novoselov, K. S. Detection of Individual Gas Molecules Adsorbed on Graphene. *Nat. Mater.* **2007**, *6*, 652–655.
- Rumyantsev, S.; Liu, G.; Shur, M. S.; Potyrailo, R. A.; Balandin, A. A. Selective Gas Sensing with a Single Pristine Graphene Transistor. *Nano Lett.* **2012**, *12*, 2294–2298.
- Vinogradov, N. A.; Schulte, K.; Ng, M. L.; Mikkelsen, A.; Lundgren, E.; Mårtensson, N.; Preobrajenski, A. B. Impact of Atomic Oxygen on the Structure of Graphene Formed on Ir(111) and Pt(111). *J. Phys. Chem. C* **2011**, *115*, 9568–9577.
- Larciprete, R.; Fabris, S.; Sun, T.; Lacovig, P.; Baraldi, A.; Lizzit, S. Dual Path Mechanism in the Thermal Reduction of Graphene Oxide. *J. Am. Chem. Soc.* **2011**, *133*, 17315–17321.
- Nair, R. R.; Ren, W.; Jalil, R.; Riaz, I.; Kravets, V. G.; Britnell, L.; Blake, P.; Schedin, F.; Mayorov, A. S.; Yuan, S.; et al. Fluorographene: A Two-Dimensional Counterpart of Teflon. *Small* **2010**, *6*, 2877–2884.
- Balog, R.; Jørgensen, B.; Nilsson, L.; Andersen, M.; Rienks, E.; Bianchi, M.; Fanetti, M.; Laegsgaard, E.; Baraldi, A.; Lizzit, S.; et al. Bandgap Opening in Graphene Induced by Patterned Hydrogen Adsorption. *Nat. Mater.* **2010**, *9*, 315–319.
- Bostwick, A.; Mcchesney, J. L.; Emtsev, K. V.; Seyller, T.; Horn, K.; Kevan, S. D.; Rotenberg, E. Quasiparticle Transformation during a Metal-Insulator Transition in Graphene. *Phys. Rev. Lett.* **2009**, *103*, 1–4.
- Ng, M. L.; Balog, R.; Hornekaer, L.; Preobrajenski, A. B.; Vinogradov, N. A.; Mårtensson, N.; Schulte, K. Controlling Hydrogenation of Graphene on Transition Metals. *J. Phys. Chem. C* **2010**, *114*, 18559–18565.
- Ryu, S.; Han, M. Y.; Maultzsch, J.; Heinz, T. F.; Kim, P.; Steigerwald, M. L.; Brus, L. E. Reversible Basal Plane Hydrogenation of Graphene. *Nano Lett.* **2008**, *8*, 4597–4602.
- Boukhvalov, D. W.; Son, Y.-W. Covalent Functionalization of Strained Graphene. *Chem. Phys. Chem.* **2012**, *13*, 1463–1469.
- Sun, Z.; Pint, C. L.; Marcano, D. C.; Zhang, C.; Yao, J.; Ruan, G.; Yan, Z.; Zhu, Y.; Hauge, R. H.; Tour, J. M. Towards Hybrid Superlattices in Graphene. *Nat. Commun.* **2011**, *2*, 559.
- Englert, J. M.; Dotzer, C.; Yang, G.; Schmid, M.; Papp, C.; Gottfried, J. M.; Steinrück, H.-P.; Spiecker, E.; Hauke, F.; Hirsch, A. Covalent Bulk Functionalization of Graphene. *Nat. Chem.* **2011**, *3*, 279–286.
- Haberer, D.; Vyalikh, D. V.; Taioli, S.; Dora, B.; Farjam, M.; Fink, J.; Marchenko, D.; Pichler, T.; Ziegler, K.; Simonucci, S.; et al. Tunable Band Gap in Hydrogenated Quasi-Free-Standing Graphene. *Nano Lett.* **2010**, *10*, 3360–3366.
- Samarakoon, D. K.; Wang, X.-Q. Tunable Band Gap in Hydrogenated Bilayer Graphene. *ACS Nano* **2010**, *4*, 4126–4130.
- Hornekaer, L.; Rauls, E.; Xu, W.; Sljivancanin, Z.; Otero, R.; Stensgaard, I.; Laegsgaard, E.; Hammer, B.; Besenbacher, F. Clustering of Chemisorbed H(D) Atoms on the Graphite(0001) Surface Due to Preferential Sticking. *Phys. Rev. Lett.* **2006**, *97*, 186102.
- Hornekaer, L.; Sljivancanin, Z.; Xu, W.; Otero, R.; Rauls, E.; Stensgaard, I.; Laegsgaard, E.; Hammer, B.; Besenbacher, F. Metastable Structures and Recombination Pathways for Atomic Hydrogen on the Graphite(0001) Surface. *Phys. Rev. Lett.* **2006**, *96*, 156104.
- Hornekaer, L.; Xu, W.; Otero, R.; Laegsgaard, E.; Besenbacher, F. Long Range Orientation of Meta-Stable Atomic Hydrogen Adsorbate Clusters on the Graphite(0001) Surface. *Chem. Phys. Lett.* **2007**, *446*, 237–242.
- Cuppen, H. M.; Hornekaer, L. Kinetic Monte Carlo Studies of Hydrogen Abstraction From Graphite. *J. Chem. Phys.* **2008**, *128*, 174707.
- Sljivancanin, Z.; Rauls, E.; Hornekaer, L.; Xu, W.; Besenbacher, F.; Hammer, B. Extended Atomic Hydrogen Dimer Configurations on the Graphite(0001) Surface. *J. Chem. Phys.* **2009**, *131*, 084706.
- Nikitin, A.; Naslund, L.; Zhang, Z.; Nilsson, A. C–H Bond Formation at the Graphite Surface Studied with Core Level Spectroscopy. *Surf. Sci.* **2008**, *602*, 2575–2580.
- Sljivancanin, Z.; Andersen, M.; Hornekaer, L.; Hammer, B. Structure and Stability of Small H Clusters on Graphene. *Phys. Rev. B* **2011**, *83*, 205426.
- Casolo, S.; Lovvik, O. M.; Martinazzo, R.; Tantardini, G. F. Understanding Adsorption of Hydrogen Atoms on Graphene. *J. Chem. Phys.* **2009**, *130*, 054704.
- Ruffieux, P.; Groning, O.; Bielmann, M.; Mauron, P.; Schlapbach, L.; Groning, P. Hydrogen Adsorption on sp^2 -Bonded Carbon: Influence of the Local Curvature. *Phys. Rev. B* **2002**, *66*, 245416.
- Park, S.; Srivastava, D.; Cho, K. Generalized Chemical Reactivity of Curved Surfaces: Carbon Nanotubes. *Nano Lett.* **2003**, *3*, 1273–1277.
- Varchon, F.; Mallet, P.; Veuillet, J. Y.; Magaud, L. Ripples in Epitaxial Graphene on the Si-Terminated SiC(0001) Surface. *Phys. Rev. B* **2008**, *77*, 235412.
- Rajasekaran, S.; Kaya, S.; Abild-Pedersen, F.; Anniyev, T.; Yang, F.; Stacchiola, D.; Ogasawara, H.; Nilsson, A. Reversible Graphene-Metal Contact through Hydrogenation. *Phys. Rev. B* **2012**, *86*, 075417.
- Feibelman, P. J. Pinning of Graphene to Ir(111) by Flat Ir Dots. *Phys. Rev. B* **2008**, *77*, 165419.
- Sun, Z.; Hämäläinen, S.; Sainio, J.; Lahtinen, J.; Vanmaekelbergh, D.; Liljeroth, P. Topographic and Electronic Contrast of the Graphene Moiré on Ir(111) Probed by Scanning Tunneling Microscopy and Noncontact Atomic Force Microscopy. *Phys. Rev. B* **2011**, *83*, 081415.
- Busse, C.; Lazić, P.; Djemour, R.; Coraux, J.; Gerber, T.; Atodiresei, N.; Caciuc, V.; Brako, R.; N'Diaye, A.; Blügel, S.; et al. Graphene on Ir(111): Physisorption with Chemical Modulation. *Phys. Rev. Lett.* **2011**, *107*, 036101.
- Sofo, J. O.; Chaudhari, A. S.; Barber, G. D. Graphane: A Two-Dimensional Hydrocarbon. *Phys. Rev. B* **2007**, *75*, 153401.
- Elias, D. C.; Nair, R. R.; Mohiuddin, T. M. G.; Morozov, S. V.; Blake, P.; Halsall, M. P.; Ferrari, A. C.; Boukhvalov, D. W.; Katsnelson, M. I.; Geim, A. K.; et al. Control of Graphene's Properties by Reversible Hydrogenation: Evidence for Graphane. *Science* **2009**, *323*, 610–613.
- Andersen, M.; Hornekaer, L.; Hammer, B. Graphene on Metal Surfaces and Its Hydrogen Adsorption: A Meta-GGA Functional Study. *Phys. Rev. B* **2012**, *86*, 085405.

39. Lacovic, P.; Pozzo, M.; Alfè, D.; Vilmercati, P.; Baraldi, A.; Lizzit, S. Growth of Dome-Shaped Carbon Nanoislands on Ir(111): The Intermediate between Carbodic Clusters and Quasi-Free-Standing Graphene. *Phys. Rev. Lett.* **2009**, *103*, 166101.
40. Pletikosic, I.; Kralj, M.; Pervan, P.; Brako, R.; Coraux, J.; N'Diaye, A.; Busse, C.; Michely, T. Dirac Cones and Minigaps for Graphene on Ir(111). *Phys. Rev. Lett.* **2009**, *102*, 056808.
41. Zecho, T.; Guttler, A.; Sha, X.; Lemoine, D.; Jackson, B.; Kuppers, J. Abstraction of D Chemisorbed on Graphite-(0001) with Gaseous H Atoms. *Chem. Phys. Lett.* **2002**, *366*, 188–195.
42. Zecho, T.; Guttler, A.; Sha, X.; Jackson, B.; Kuppers, J. Adsorption of Hydrogen and Deuterium Atoms on the (0001) Graphite Surface. *J. Chem. Phys.* **2002**, *117*, 8486–8492.
43. Kim, H.; Balgar, T.; Hasselbrink, E. The Stretching Vibration of Hydrogen Adsorbed on Epitaxial Graphene Studied by Sum-Frequency Generation Spectroscopy. *Chem. Phys. Lett.* **2011**, *508*, 1–5.
44. Enkovaara, J.; Rostgaard, C.; Mortensen, J. J.; Chen, J.; Dulak, M.; Ferrighi, L.; Gavnholt, J.; Glinsvad, C.; Haikola, V.; Hansen, H. A.; *et al.* Electronic Structure Calculations with GPAW: A Real-Space Implementation of the Projector Augmented-Wave Method. *J. Phys.: Condens. Matter* **2010**, *22*, 253202.
45. Perdew, J. P.; Burke, K.; Ernzerhof, M. Generalized Gradient Approximation Made Simple. *Phys. Rev. Lett.* **1996**, *77*, 3865–3868.
46. Zhao, Y.; Truhlar, D. G. A New Local Density Functional for Main-Group Thermochemistry, Transition Metal Bonding, Thermochemical Kinetics, and Noncovalent Interactions. *J. Chem. Phys.* **2006**, *125*, 194101.
47. N'Diaye, A. T.; Coraux, J.; Plasa, T. N.; Busse, C.; Michely, T. Structure of Epitaxial Graphene on Ir(111). *New J. Phys.* **2008**, *10*, 043033.